Electronic Supplementary Material (ESI) for Dalton Transactions

Cyclometalated Heteronuclear Pt/Ag and Pt/Tl Complexes: A Structural and Photophysical Study

Sirous Jamali,[a] Reza Ghazfar,[a] Elena Lalinde,[b] Zahra Jamshidi,[c] Hamidreza Samouie,[d] Hamid R. Shahsavari,[b] M. Teresa Moreno,[b] Eduardo Escudero-Adán,[d] J. Benet-Buchholz[d]*

[a]Chemistry Department, Sharif University of Technology, Tehran, P.O. Box 11155-3516, Iran; [b]Departamento de Química-Centro de Síntesis Química de La Rioja, (CISQ), Universidad de La Rioja, 26006, Logroño, Spain; [c]Chemistry and Chemical Engineering Research Center of Iran, Tehran, Iran; [d]Institute of Chemical Research of Catalonia (ICIQ), Avgda. PaïsosCatalans 16, 43007 Tarragona, Spain

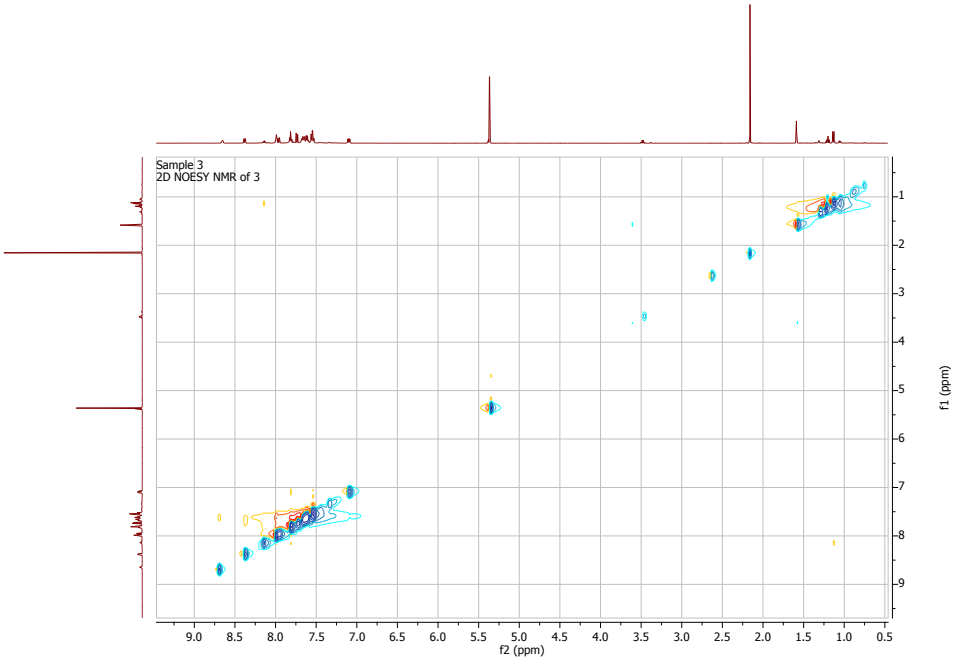

Figure S1. 2D ^{1}H-^{1}H NOESY NMR spectrum of **3** in CD_2Cl_2

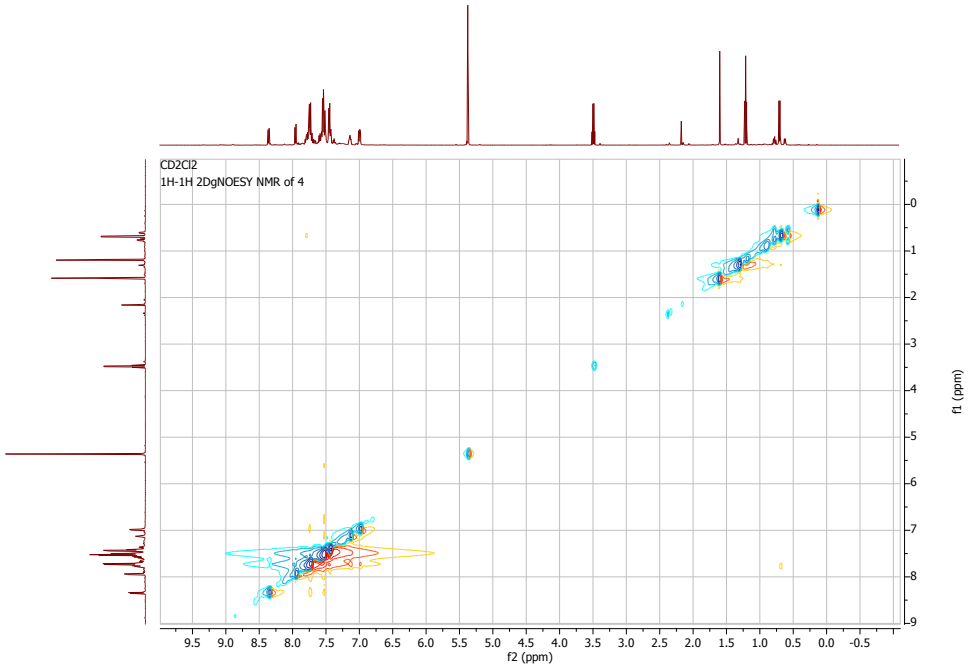

Figure S2. 2D ^{1}H-^{1}H NOESY NMR spectrum of **4** in CD_2Cl_2

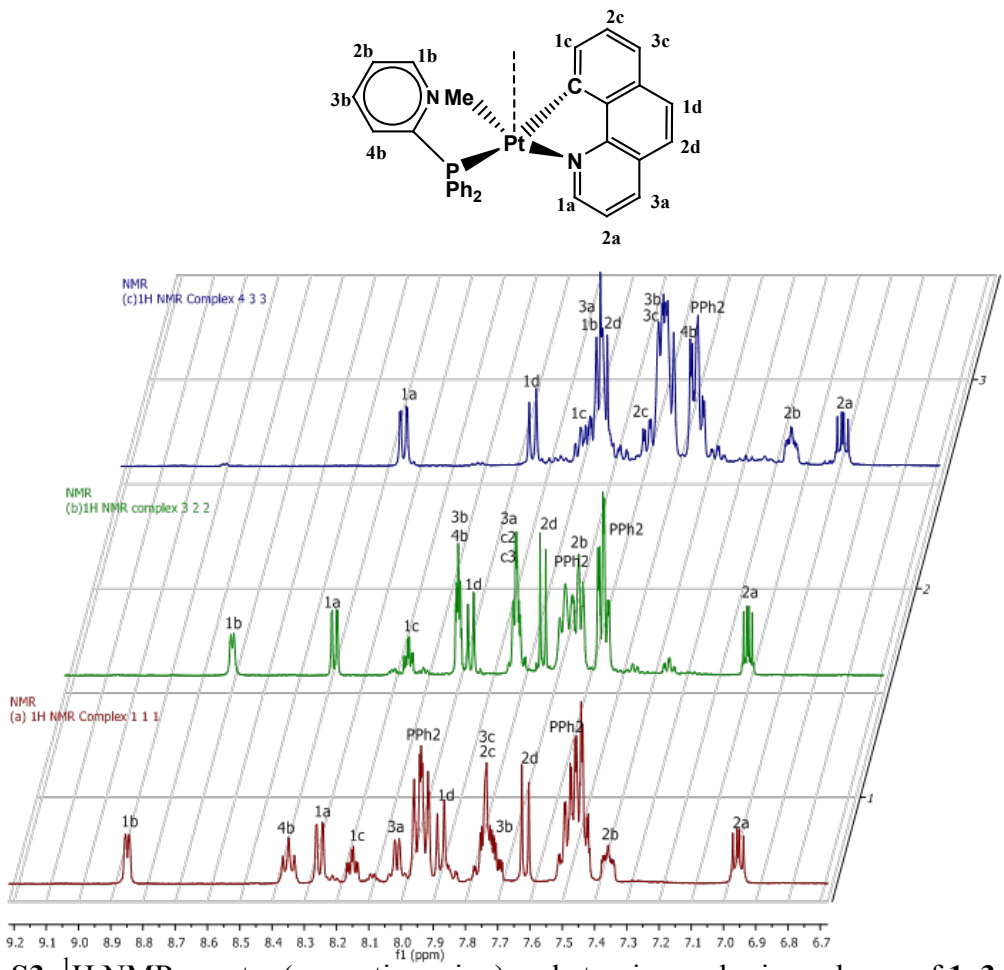

Figure S3. ^{1}H NMR spectra (aromatic region) and atomic numbering scheme of **1**, **3** and **4**

Four distinct sets of correlations observed in the COSY-DQF spectra of **1**, **3** (Figures S4 and S5). The first set delineating the sequence from the protons of the CH groups adjacent to the N atoms of the bhq ligands, H1a protons (δ_1= 8.25 and δ_3=8.38 ppm) and extending through the H2a protons (δ_1=6.9 and δ_3=7.1 ppm) and the H3a protons (δ_1= 8 and δ_3=7.8 ppm). Remarkably, H2a protons, directed toward the face of the phenyl ring of dppy ligands, are shielded by the ring-current effect of the phenyl rings (Figure S6 in SI). A second set of correlations defined the sequence from the CH groups adjacent to the N atoms of the dppy ligands, H1b protons (δ_1= 8.85 and δ_3=8.69 ppm) through to the H2b protons (δ_1= 7.36 and δ_3=7.61 ppm) and extending through the H3b protons (δ_1= 7.7 and δ_3=8 ppm) and terminating at the H4b protons (δ_1= 8.35 and δ_3=8 ppm). A third comparable set of correlations established the sequence from the CH groups adjacent to the C atoms of the bhq ligands, H1c protons (δ_1 and δ_3= 8.15 ppm) through the H2c protons (δ_1=7.74 and δ_3=7.81 ppm) to the H3c protons (δ_1= 7.74 and δ_3=7.81 ppm). An additional set of correlations were detected between H1d protons (δ_1=7.87 and δ_3=7.95 ppm) and H2d protons(δ_1=7.62 and δ_3=7.73 ppm). Furthermore, the COSY-LR NMR spectra of **1** and **3** (Figure S7) reveal long range correlation of H1d and H2d protons with (H1c, H2c,H3c) and (H1a, H2a, H3a) proton sets respectively. Chemical shifts for phenyl protons of the PPh_2 groups

are clustered at 7.5 and 8 ppm. The trinuclear complex **4** showed similar ^{1}H NMR, COSY-DQF and COSY-LR (Figure S8 and S9) pattern with complexes **1** and **3**. However, two protons set (H1c-3c) and (H1b-4b) showed a large upfield shift in the ^{1}H NMR spectrum of **4** in comparison with those observed in the ^{1}H NMR spectra of **1** and **3**. The up-field shifts of the (H1b-4b) and (Hc1-3c) protons in **4** have been ascribed to the shielding from the ring current of the bhq ligand of the second [PtMe(bhq)(dppy)] and the phenyl rings of PPh_2 units. The upfield movement of aromatic signals and specially resonances of the H1b-H4b protons supports the formation of trinuclear complex **4** with the same conformation as that predicted by DFT calculations and shown in Figure S16.

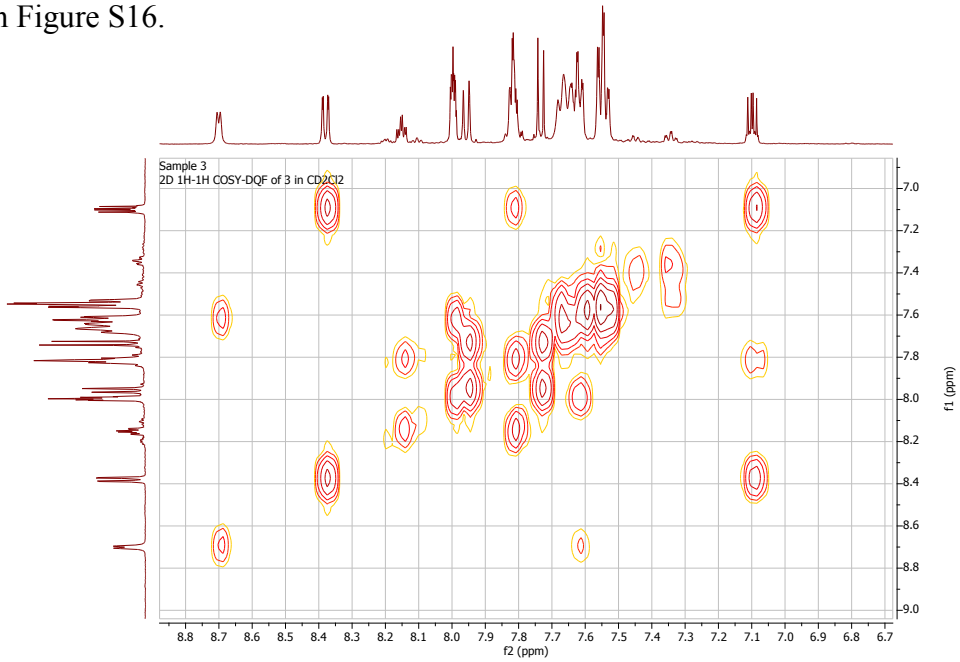

Figure S4. 2D ^{1}H-^{1}H COSY-DQF NMR spectrum of **3** in CD_2Cl_2(aromatic region)

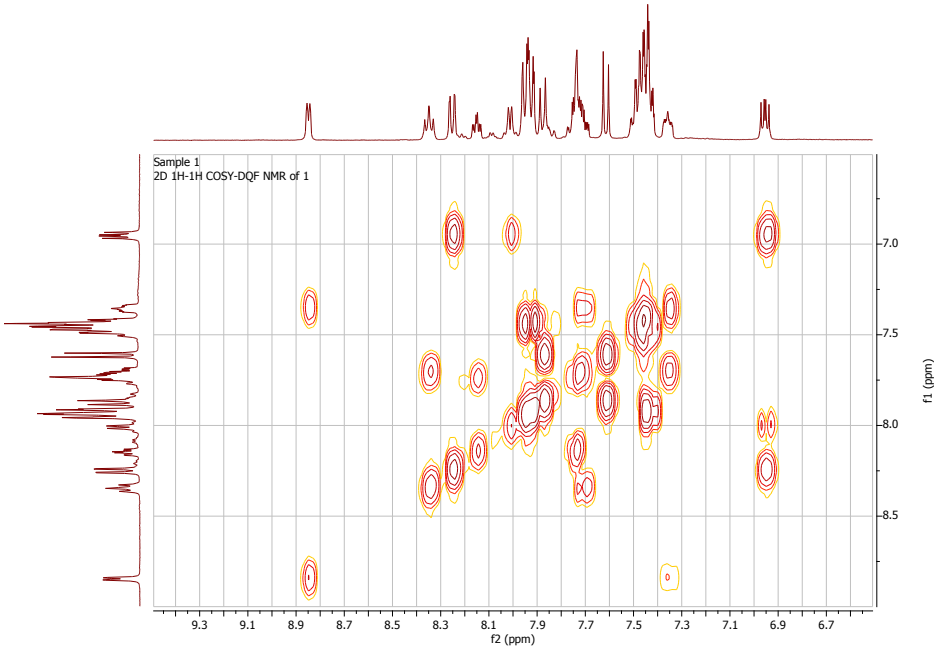

Figure S ic region)

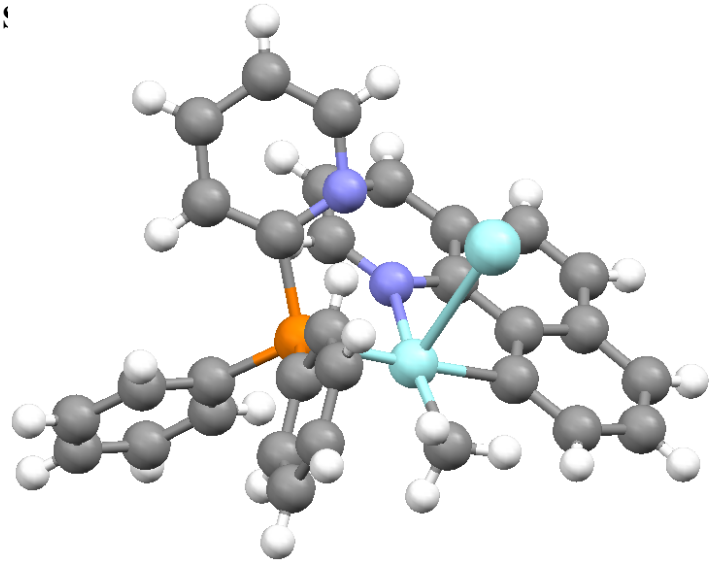

Figure S6. Crystal structure of **3** that shows H2a directed toward the face of the pyridyl ring of dppy ligands

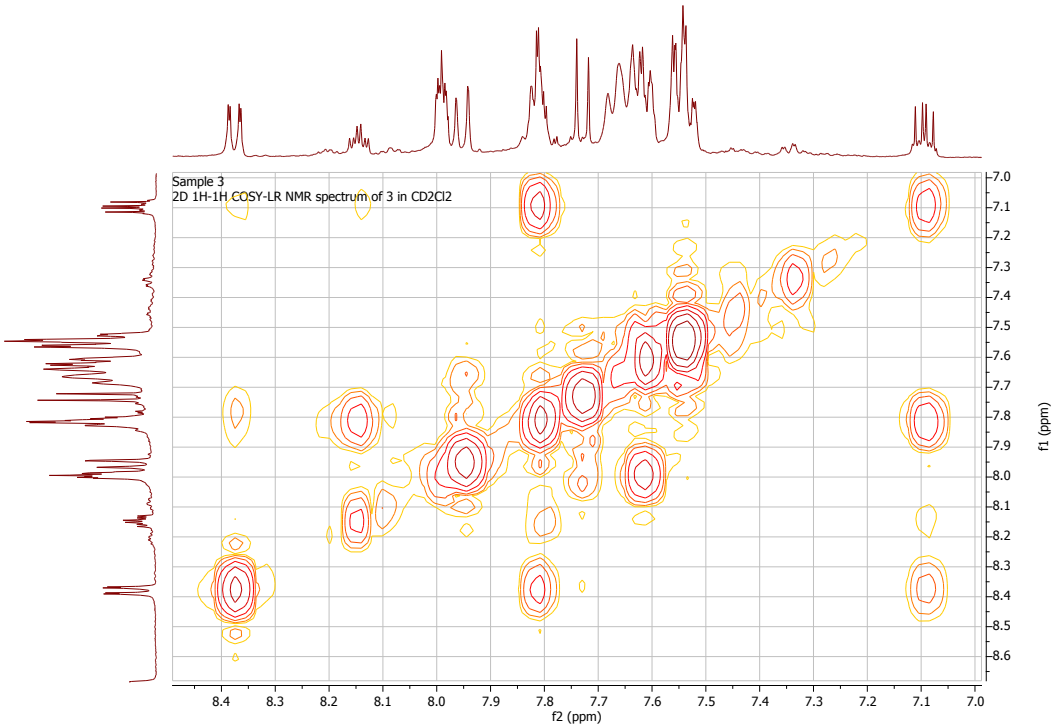

Figure S7. 2D ^{1}H-^{1}H COSY-LR NMR spectrum of **3** in CD_2Cl_2 (aromatic region)

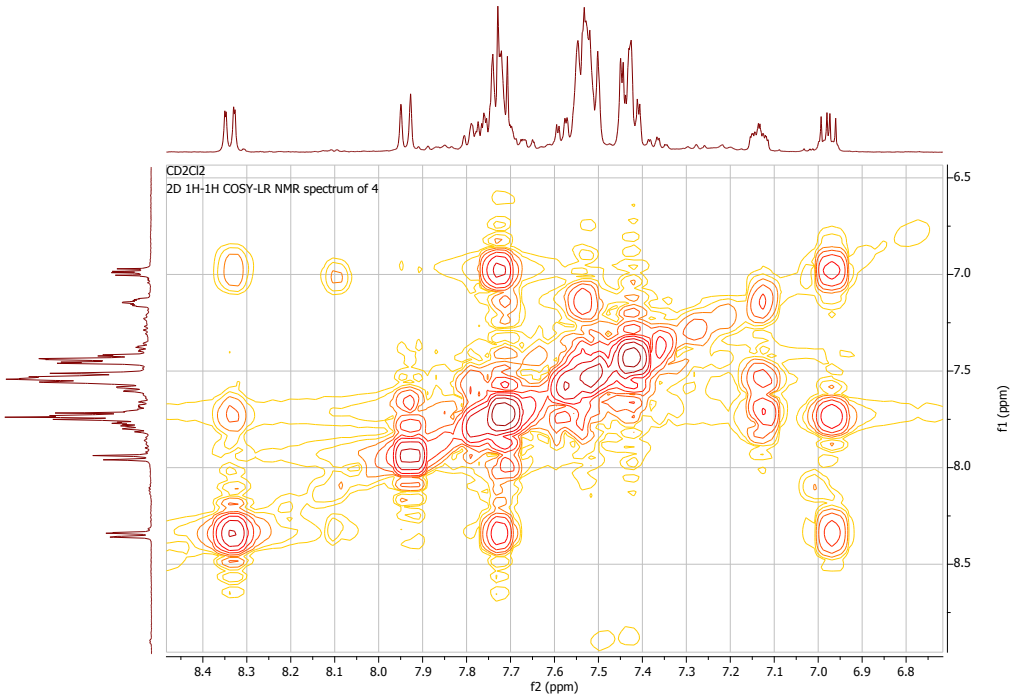

Figure S8. 2D ^{1}H-^{1}H COSY-LR NMR spectrum of **4** in CD_2Cl_2 (aromatic region)

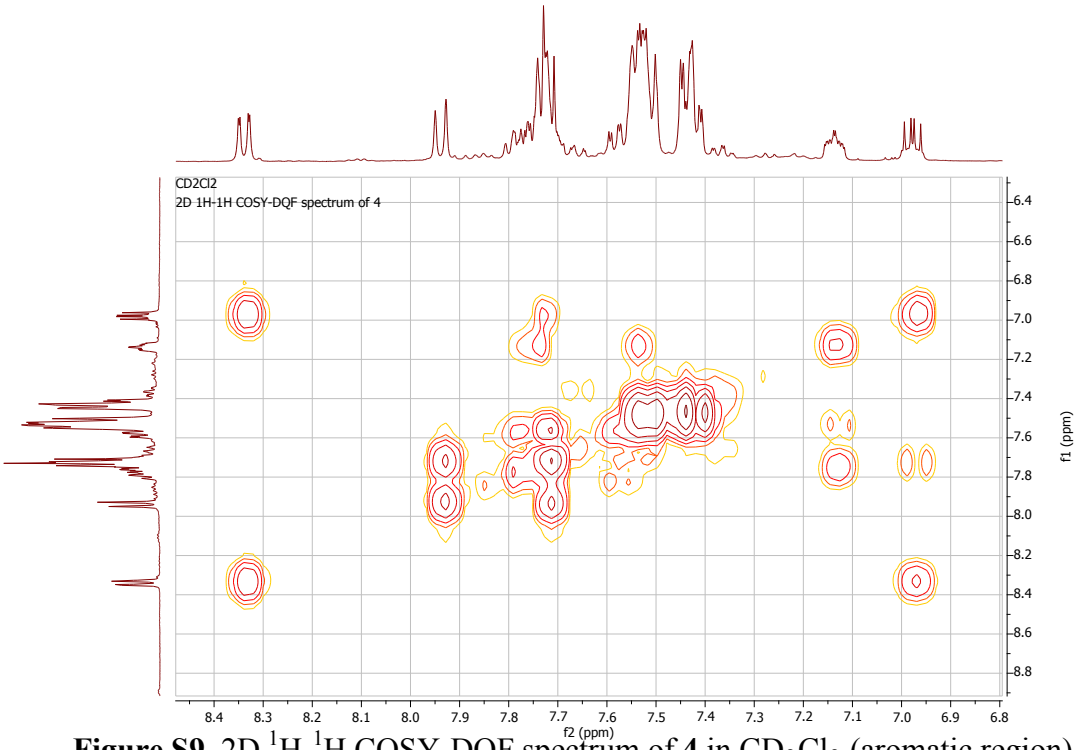

Figure S9. 2D ^{1}H-^{1}H COSY-DQF spectrum of **4** in CD_2Cl_2 (aromatic region)

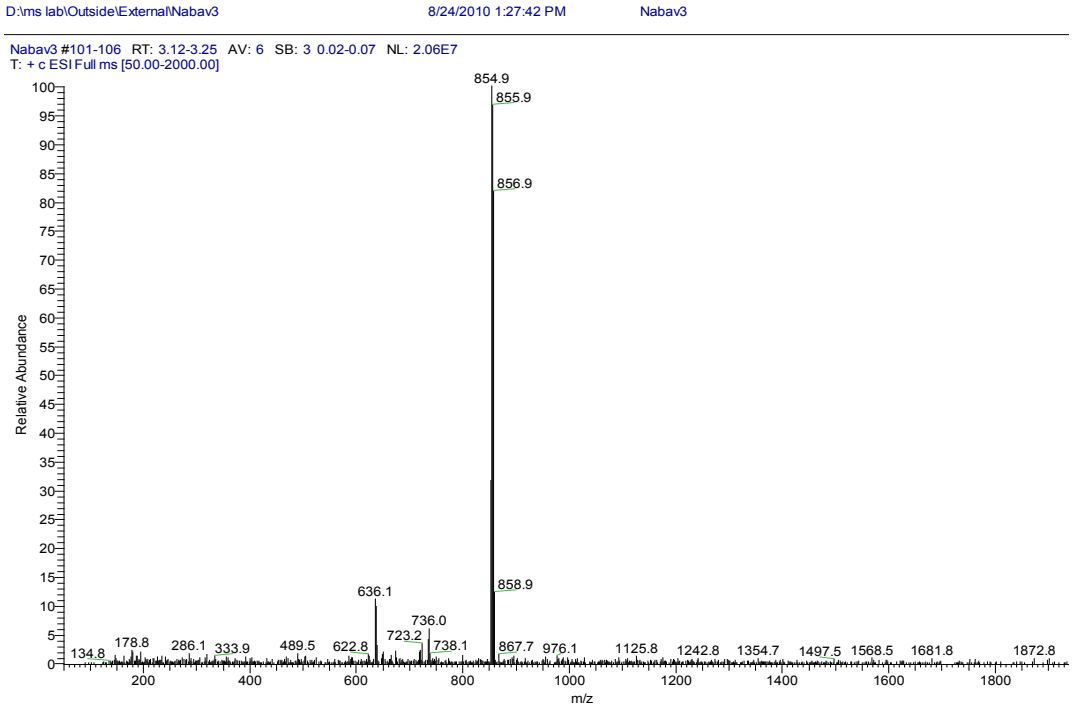

Figure S10. ESI-Mass spectrum (positive ion mode) of **3**

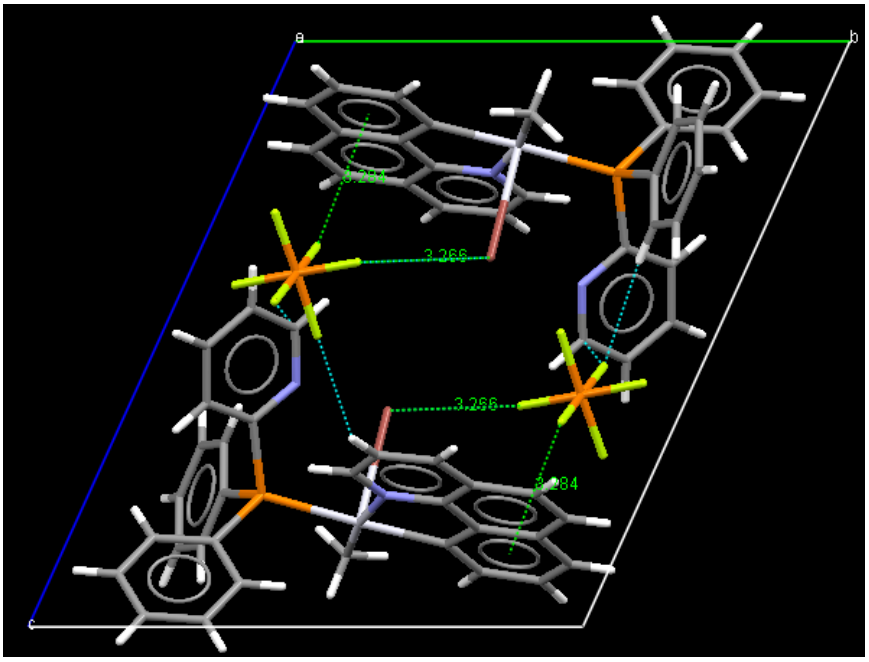

Figure S11. Extended network of **3** showing the Tl···F interactions (3.236 Å)

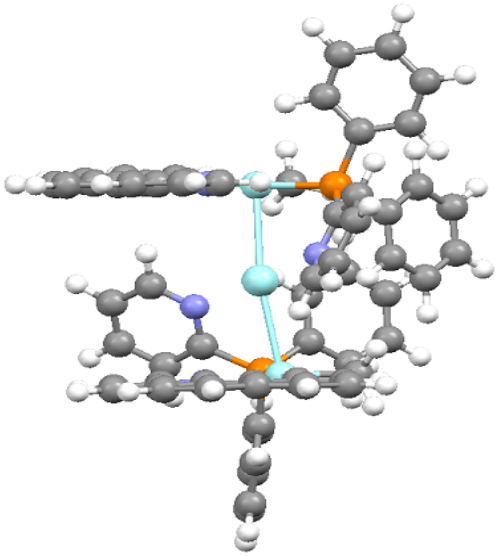

Figure S12. Optimized structure of trinuclear Pt-Tl-Tl complex **4** showing positions of the H1c and H2c protons in the ring current of bhq ligands

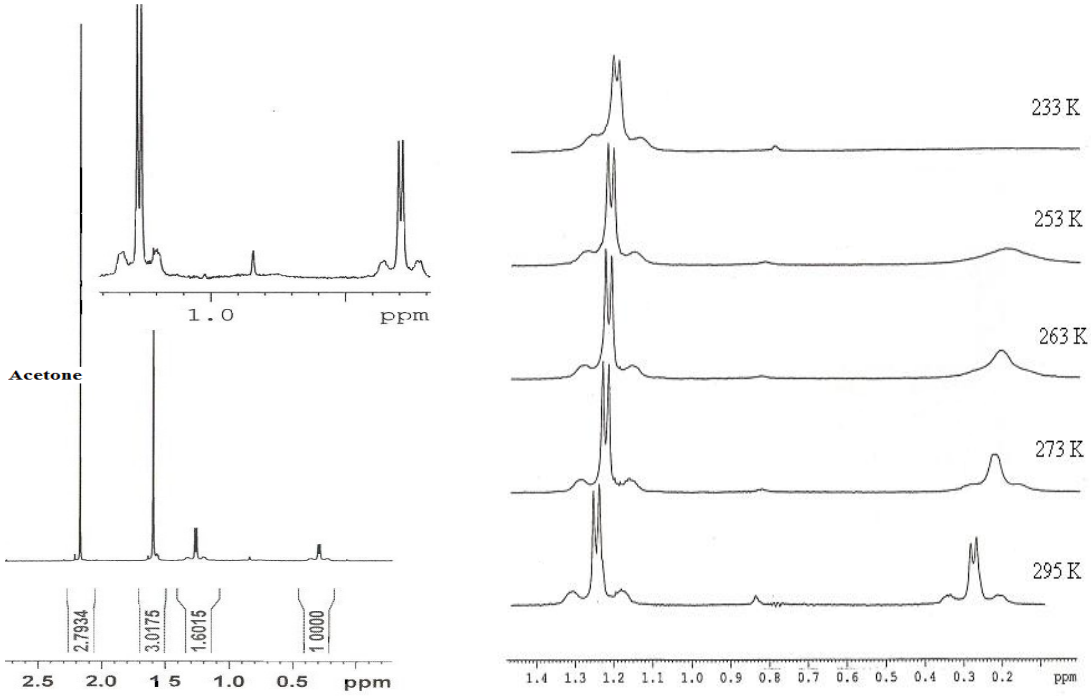

Figure S13. Left: ^{1}H NMR spectrum of single crystals of **2** in $CDCl_3$ shows removing acetone molecule Right: VT-^{1}H NMR spectrum of **2** in $CDCl_3$.

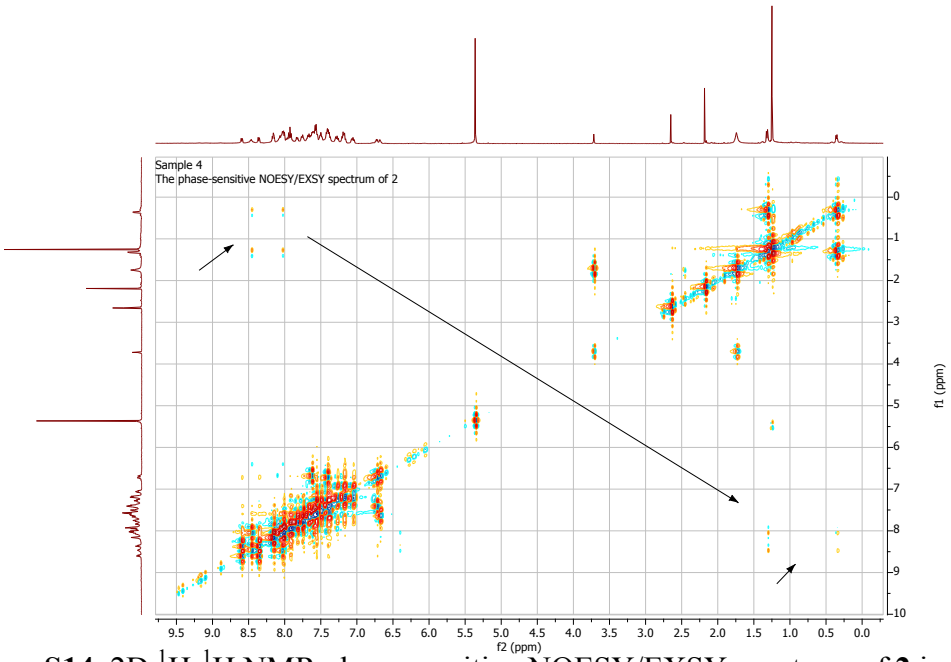

Figure S14. 2D ^{1}H-^{1}H NMR phase-sensitive NOESY/EXSY spectrum of **2** in CD_2Cl_2

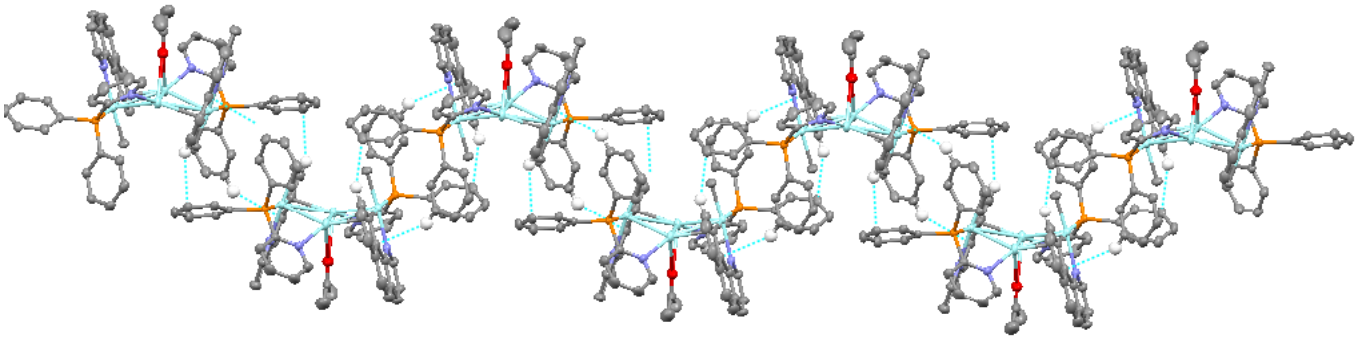

Figure S15. Extended molecular structure of **2**. The BF_4 counter-ions are omitted for clarity

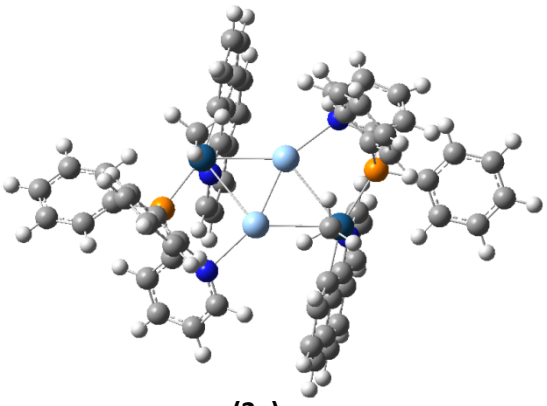

(2a)

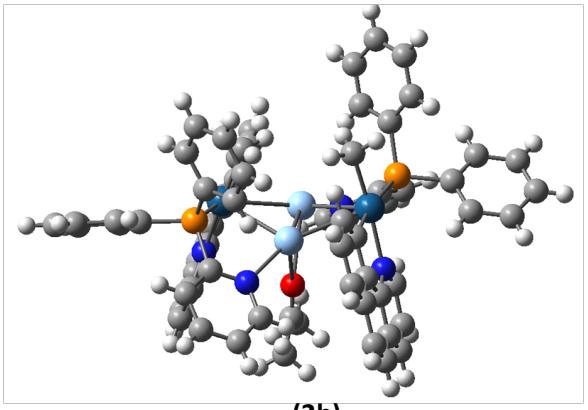

(2b)

Figure S16. Optimized structure of complex **2** (**2a**) and (**2b**) Structure based on cif crystallographic data

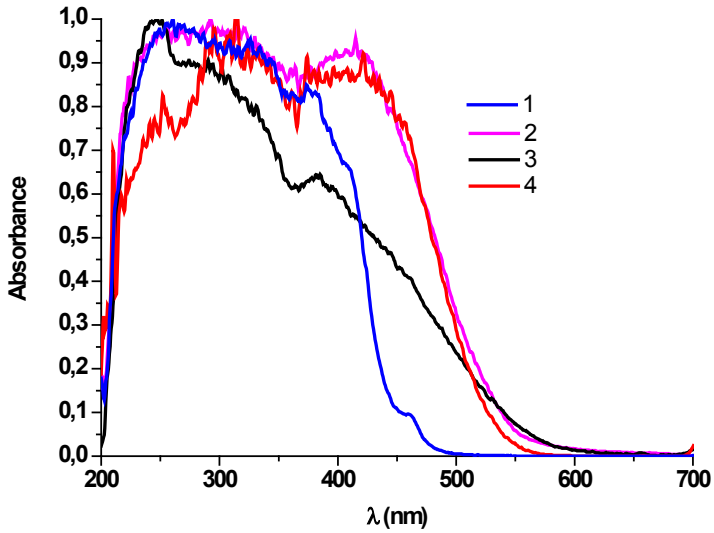

Figure S17. Normalized diffuse reflectance UV-vis spectra of **1-4** in the solid state

Table S1. Calculated Energy and Compositions of the Electronic Transitions of Complex $[Pt_2Me_2(bhq)_2(\mu\text{-dppy})_2Ag_2](BF_4)_2$ (**2**)

state	Composition	λ (calc.)/nm	f
S_1	HOMO-1→LUMO (95%)	514	0.0018
S_2	HOMO→LUMO (60%), HOMO-1→LUMO(34%)	449	0.0244
S_3	HOMO-2→LUMO (98%)	412	0.0444
S_4	HOMO-3→LUMO (3%), HOMO-1→LUMO+1 (84%), HOMO-1→LUMO+2 (8%)	402	0.0012
S_5	HOMO-4→LUMO+1 (12%), HOMO-3→LUMO (81%), HOMO-1→LUMO+1 (3%)	399	0.0078
S_6	HOMO→LUMO+1 (99%)	385	0.0018
S_7	HOMO-6→LUMO (4%), HOMO-4→LUMO (77%), HOMO-3→LUMO (14%)	368	0.0347
S_8	HOMO-7→LUMO (3%), HOMO-5→LUMO (93%)	363	0.0196
T_1	HOMO-1→LUMO (70%), HOMO→LUMO (26%)	549	0.0000
T_2	HOMO→LUMO (98%)	458	0.0000
T_3	HOMO-2→LUMO (81%), HOMO-1→LUMO+1 (9%)	421	0.0000
T_4	HOMO-3→LUMO (3%), HOMO-2→LUMO (15%), HOMO-1→LUMO+1 (62%), HOMO-1→LUMO+2 (11%)	415	0.0000
T_5	HOMO-4→LUMO (18%), HOMO-3→LUMO (68%), HOMO-1→LUMO+1 (6%)	407	0.0000

T_6	HOMO-7→LUMO (6%), HOMO-4→LUMO (6%), HOMO-3→LUMO (4%), HOMO→LUMO+1 (72%)	389	0.0000
T_7	HOMO-9→LUMO (5%), HOMO-8→LUMO (6%), HOMO-7→LUMO (18%), HOMO-5→LUMO (7%), HOMO-4→LUMO (17%), HOMO-3→LUMO (15%), HOMO→LUMO+1 (24%)	387	0.0000
T_8	HOMO-9→LUMO (3%), HOMO-7→LUMO (7%), HOMO-5→LUMO (46%), HOMO-4→LUMO (37%), HOMO-3→LUMO+7 (5%)	374	0.0000

Table S2. Calculated Energy and Compositions of the Electronic Transitions of Complex [PtMe(bhq)(dppy)Tl]PF_6 (**3**)

state	composition	λ (calc.)/nm	f
S_1	HOMO→LUMO (65%), HOMO→LUMO+1 (31%)	398	0.0374
S_2	HOMO→LUMO (29%), HOMO→LUMO+1 (64%), HOMO→LUMO+2 (6%)	388	0.0077
S_3	HOMO→LUMO (5%), HOMO→LUMO+1 (91%)	357	0.0022
S_4	HOMO-1→LUMO (35%), HOMO-1→LUMO+1 (40%), HOMO→LUMO+3 (17%), HOMO→LUMO+4 (4%)	345	0.0033
S_5	HOMO-1→LUMO (56%), HOMO-1→LUMO+1 (27%), HOMO-1→LUMO+2 (4%), HOMO→LUMO+3 (8%)	331	0.0056
S_6	HOMO-3→LUMO (4%), HOMO-2→LUMO (77%), HOMO-2→LUMO+1 (6%), HOMO-2→LUMO+2 (7%)	326	0.0095
S_7	HOMO-5→LUMO+1 (2%), HOMO-2→LUMO+1 (4%), HOMO-1→LUMO+1 (21%), HOMO→LUMO+3 (59%), HOMO→LUMO+5 (3%)	323	0.0822
S_8	HOMO→LUMO+3 (4%), HOMO→LUMO+4 (90%)	319	0.0097
T_1	HOMO→LUMO+3 (36%), HOMO-1→LUMO+1 (28%), HOMO→LUMO+4 (10%), HOMO→LUMO+6 (5%), HOMO→LUMO+5 (4%), HOMO-1→LUMO (4%)	467	0.0000
T_2	HOMO→LUMO (25%), HOMO→LUMO+1 (65%)	456	0.0000
T_3	HOMO→LUMO (48%), HOMO→LUMO+1 (18%), HOMO-1→LUMO+1 (15%), HOMO→LUMO+2 (6%), HOMO→LUMO+3 (4%), HOMO-1→LUMO (3%)	394	0.0000
T_4	HOMO-1→LUMO (11%), HOMO-1→LUMO+1 (29%), HOMO→LUMO (16%), HOMO→LUMO+1 (7%), HOMO→LUMO+3 (19%), HOMO→LUMO+4 (4%)	388	0.0000
T_5	HOMO-2→LUMO+1 (31%), HOMO-2→LUMO (28%), HOMO-3→LUMO+1 (9%), HOMO-3→LUMO (9%), HOMO-2→LUMO+3 (7%), HOMO-2→LUMO+4 (3%), HOMO-3→LUMO+3 (3%)	370	0.0000
T_6	HOMO-2→LUMO (3%), HOMO→LUMO (9%), HOMO→LUMO+2 (80%)	361	0.0000
T_7	HOMO-2→LUMO+1 (24%), HOMO-2→LUMO+2 (21%), HOMO-2→LUMO (20%), HOMO-3→LUMO (7%), HOMO-3→LUMO+2 (7%), HOMO→LUMO+2 (7%), HOMO-3→LUMO+1 (7%)	347	0.0000
T_8	HOMO-3→LUMO+8 (20%), HOMO-4→LUMO+10 (10%), HOMO-4→LUMO+9 (8%), HOMO-2→LUMO+8 (7%), HOMO-8→LUMO+7 (4%), HOMO-10→LUMO+8 (4%), HOMO-7→LUMO+10 (3%), HOMO-8→LUMO+5 (3%), HOMO-4→LUMO+1 (3%), HOMO-3→LUMO (3%), HOMO-3→LUMO+2 (3%)	342	0.0000

Table S3. Crystal Data and Structure Refinement Parameters for Complex **3**

Empirical formula	$C_{31}H_{25}N_2PPtTl.PF_6.H_2O$
Formula mass	1018.95
Crystal size (mm)	0.25 × 0.20 × 0.04
Colour	yellow-orange
Crystal system	triclinic
Space group	*P-1*
θ_{max} (°)	30.0
a (Å)	9.1552(3)
b (Å)	13.2850(5)
c (Å)	14.9645(6)
α (°)	109.037(3)
β (°)	101.241(3)
γ (°)	108.052(3)
V (Å^3)	1544.58(12)
Z	2
D_{calc} (Mg/m^3)	2.191
μ (mm^{-1})	9.902
F(000)	956
Index ranges	$-12 \leq h \leq 12$
	$-18 \leq k \leq 18$
	$-21 \leq l \leq 21$
No. of measured	18299
reflections	8881/0.029
No. of independent	
reflections/R_{int}	7029
No. of observed	399
reflections with $I > 2\sigma(I)$	0.95
No. of parameters	0.0296
Goodness-of-fit (GOF)	0.0727
R_1 (observed data)	

wR_2 (all data)[a]
$w = 1/[\sigma^2(F_o^2)+(0.0447P)^2 + 32.1161P]$ for **3** in which $P = (F_o^2 + 2F_c^2)/3$

Table S4. Crystal data and structure refinement for complex **1**

Empirical formula	C31 H25 N2 P Pt	
Formula weight	651.59	
Temperature	100(2) K	
Wavelength	0.71073 Å	
Crystal system	Monoclinic	
Space group	P2(1)/n	
Unit cell dimensions	a = 24.1753(9) Å	α= 90.00 °.
	b = 9.7937(4) Å	β = 90.584(2) °.
	c = 31.2016(12) Å	γ = 90.00 °.
Volume	7387.1(5) $Å^3$	
Z	12	
Density (calculated)	1.758 Mg/m^3	
Absorption coefficient	5.787 mm^{-1}	
F(000)	3816	
Crystal size	0.12 x 0.04 x 0.03 mm^3	
Theta range for data collection	1.06 to 29.77 °.	
Index ranges	-32 <=h<=33 ,-12 <=k<=13 ,-41 <=l<=43	
Reflections collected	59916	
Independent reflections	19140 [R(int) = 0.0370]	
Completeness to theta =29.77 °	90.7%	
Absorption correction	Empirical	
Max. and min. transmission	0.8455 and 0.5435	
Refinement method	Full-matrix least-squares on F^2	
Data / restraints / parameters	19140 / 546 / 1111	
Goodness-of-fit on F^2	1.135	
Final R indices [I>2sigma(I)]	R1 = 0.0585 , wR2 = 0.1253	
R indices (all data)	R1 = 0.0827 , wR2 = 0.1347	

Largest diff. peak and hole	5.597 and -4.383 e.Å^{-3}

Complex	**3**	**2**
HOMO-1	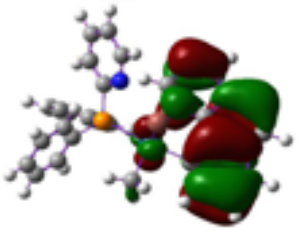	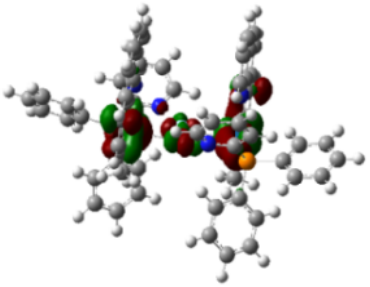
HOMO	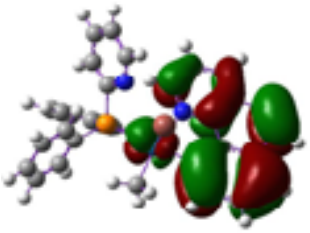	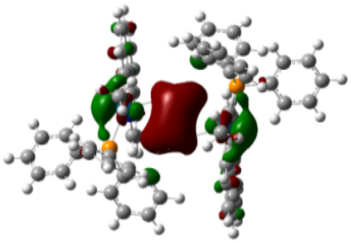
LUMO	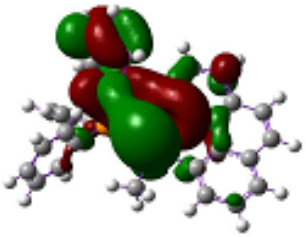	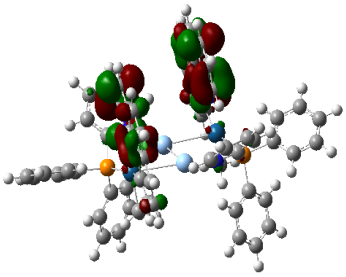
LUMO+1	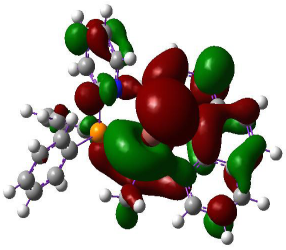	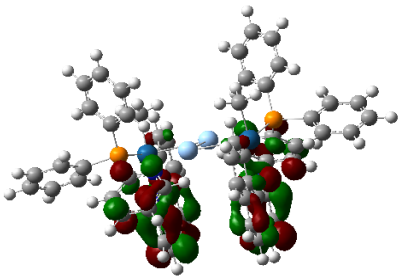

Figure S18. Selected HOMOs and LUMOs orbital plot for **2** and **3**.

Table S5. Composition (%) of frontier MOs in the ground state for complex **2**.

MO	Pt(1)	Pt(2)	Ag(1)	Ag(2)	dppy(1)	dppy(2)	bhq(1)	bhq(2)
LUMO+5	4	4	4	3	41	38	3	3
LUMO+4	8	8	3	3	9	9	29	29
LUMO+3	3	3	2	2	31	31	14	14
LUMO+2	3	3	3	3	39	39	5	5
LUMO+1	4	4	5	5	16	15	25	26
LUMO	4	4	6	6	6	5	36	35
HOMO	12	12	19	19	10	10	8	8
HOMO-1	19	19	9	9	8	8	14	14
HOMO-2	17	17	3	3	6	6	24	24
HOMO-3	33	33	8	8	1	1	6	6
HOMO-4	22	22	8	8	3	3	16	16
HOMO-5	29	29	1	1	2	2	15	14

Table S6. Composition (%) of Frontier MOs in the ground state for complex **3**.

MO	Pt(1)	Pt(2)	Ag(1)	Ag(2)	dppy(1)	dppy(2)	bhq(1)	bhq(2)
LUMO+5	4	4	4	3	41	38	3	3
LUMO+4	8	8	3	3	9	9	29	29
LUMO+3	3	3	2	2	31	31	14	14
LUMO+2	3	3	3	3	39	39	5	5
LUMO+1	4	4	5	5	16	15	25	26
LUMO	4	4	6	6	6	5	36	35
HOMO	12	12	19	19	10	10	8	8
HOMO-1	19	19	9	9	8	8	14	14
HOMO-2	17	17	3	3	6	6	24	24
HOMO-3	33	33	8	8	1	1	6	6
HOMO-4	22	22	8	8	3	3	16	16
HOMO-5	29	29	1	1	2	2	15	14

Table S7. TD-DFT Calculated energy levels and experimental absorption spectra parameters of **2** and **3**.

	Calculated					Experimental (CH_2Cl_2)
Complex	state	λ_{max}[nm]	f	Assignments	nature	λ_{max}[nm]
2	S_1	514	0.0018	HOMO-1-> LUMO (95%)		
	S_2	449	0.0244	HOMO-> LUMO (60%) HOMO-1->LUMO (34%)	^{1}MM'LCT/ ^{1}L'LCT	413
	T_1	549	0.0000	HOMO-1-> LUMO (70%) HOMO-> LUMO (26%)		
3	S_1	398	0.0374	HOMO-> LUMO (65%) HOMO-> LUMO+1 (31%)	^{1}LL'CT/ ^{1}LM'CT	404
	S_2	388	0.0077	HOMO->LUMO (29%) HOMO ->LUMO+1 (64%)	^{1}LL'CT/ ^{1}LM'CT	378
	T_1	467	0.0000	HOMO-> LUMO+3 (38%) HOMO-1> LUMO+1 (28%)		